GEOLOŠKI ANALI BALKANSKOGA POLUOSTRVA
Volume 86 (1), July 2025, 121–143
–
https://doi.org/10.2298/GABP250417005P
Original scientific paper
Оригинални научни рад

The Purpri Fault: A Newly Identified Active Fault in East Kolaka, Indonesia, Based on HypoDD and DInSAR

Joshua Purba[1*], Ramadhan Priadi[1], Muhammad Frando[2] & Imanuela Indah Pertiwi[3]

Abstract. The Purpri Fault, a newly identified active fault in East Kolaka, Indonesia, has been analyzed using an integrated geophysical approach, combining HypoDD earthquake relocation and DInSAR ground deformation analysis. The relocation of 233 seismic events from January 24 to February 7, 2025, revealed a fault structure distinct from the Middle Kolaka and North Kolaka Faults, characterized by an oblique-normal faulting mechanism with a left-lateral component. The focal mechanism solution confirms significant vertical displacement, indicating a fault that accommodates both extensional and shear deformation. DInSAR analysis using Sentinel-1A SAR imagery detected subsidence and uplift patterns that align with the relocated seismicity, confirming ongoing crustal deformation along the Purpri Fault. The western block of the fault exhibits a subsidence of approximately –13 cm, while the eastern block shows uplift of +11 cm, consistent with the seismic activity. The integration of seismic relocation and deformation mapping interpretation confirms that the Purpri Fault is an independent and active fault system. The shallow depth of seismicity (<10 km) and evidence of ongoing deformation indicate a potential seismic hazard that is not currently accounted for in regional seismic hazard models. Given its capacity to generate moderate to strong earthquakes, incorporating the Purpri Fault into updated seismic risk assessments is essential for improving earthquake preparedness and hazard mitigation strategies in East Kolaka.

Key words:
Purpri Fault, HypoDD, DInSAR, East Kolaka.

Апстракт. Расед Purpri, новоидентификовани активни расед у источној Колаки, Индонезија, анализиран је коришћењем интегрисаног геофизичког приступа, комбинујући HypoDD релокацију земљотреса и DInSAR анализу деформације тла. Релокација 233 сеизмичка догађаја од 24. јануара до 7. фебруара 2025. године открила је структуру раседа различиту од раседа Средње Колаке и Северне Колаке, коју карактерише косонормални механизам раседа са левостраном компонентом. Решење фокалног механизма потврђује значајно вертикално померање, што указује на расед са екстензионалним и смицајним деформацијама. DInSAR анализа коришћењем Sentinel-1A SAR снимака открила је обрасце

[1] Gowa Geophysical Station, Agency for Meteorology Climatology and Geophysics (BMKG), Gowa, Indonesia; E-mail: joshua.purba@bmkg.go.id
[2] Bandung Geophysical Station, Agency for Meteorology, Climatology and Geophysics (BMKG), Bandung, Indonesia
[3] Kendari Geophysical Station, Agency for Meteorology, Climatology and Geophysics (BMKG), Kendari, Indonesia

слегања и издизања који се поклапају са релоцираном сеизмичношћу, потврђујући континуирану деформацију коре дуж Purpri раседа. Западни блок раседа показује слегање од приближно -13 cm, док источни блок показује издизање од +11 cm, што је у складу са сеизмичком активношћу. Интеграција сеизмичке релокације и интерпретације мапирања деформација потврђује да је Purpri расед независан и активан систем раседа. Мала дубина сеизмичности (<10 km) и докази о континуираној деформацији указују на потенцијалну сеизмичку опасност која тренутно није узета у обзир у регионалним моделима сеизмичке опасности. С обзиром на његову способност да генерише умерене до јаке земљотресе, укључивање Purpri раседа у ажуриране процене сеизмичког ризика је неопходно за побољшање припремљености за земљотресе и стратегија за ублажавање опасности у Источној Колаки.

Кључне речи:
расед Purpri, HypoDD, DInSAR, Источна Kolaka.

Introduction

Tectonic activity in Indonesia is governed by complex geological interactions, making the region one of the most seismically active zones in the world (Hall, 2002; Hutchings & Mooney, 2021; Irsyam et al., 2020; PuSGeN, 2017; PuSGeN, 2022; PuSGeN, 2024). East Kolaka (Fig. 1), in particular, is traversed by several local fault segments (Fig. 2a-b), including the Middle Kolaka, North Kolaka, and Pelosika faults, which contribute to significant seismic hazards (PuSGeN, 2024; Soehaimi et al., 2022; Purba et al., 2024b; Simandjuntak et al., 1993; Surono & Bachri, 2002; Surono, 2010, 2013; Natawidjaja, 2021; Serhalawan & Chen, 2024; Watkinson & Hall, 2017; White et al., 2014). The presence of these faults creates a dynamic geological environment where fault interactions and segmentation play a crucial role in regional seismicity (Scholz, 2019; Philibosian & Meltzner, 2020). The identification of new active faults in this region is essential for improving earthquake hazard assessment and risk mitigation strategies (Irsyam et al., 2020; Purba et al., 2024b).

A significant tectonic earthquake occurred on January 24, 2025, in East Kolaka, Southeast Sulawesi, Indonesia, with an initial moment magnitude (Mw) of 4.9. The epicenter was located at southwest Kolaka with depth of 10 km (Fig. 1a). Following this event, three additional earthquakes were recorded on January 29, 2025: a magnitude 5.1 earthquake at a depth of 10 km, a magnitude 4.3 earthquake at a depth of 5 km, and a magnitude 4.7 earthquake at a depth of 5 km (Fig. 1b–d). Until February 7, 2025, observations from the BMKG Geophysical Station in Gowa recorded a total of 233 earthquake events (Fig. 2b,c). It's shakemap revealed that the impact could cause damage in areas close to the epicenter (BPBD, 2025).

Recent advances in geophysical techniques have made it possible to detect and characterize active faults. HypoDD (hypocenter double-difference) and Differential Interferometric Synthetic Aperture Radar (DInSAR) data have been widely applied in fault studies (Supendi et al., 2019, 2022, 2023; Fang et al., 2019; Purba et al., 2024a). These techniques provide complementary insights into fault dynamics and permit more accurate mapping of fault structures and associated seismic hazards. The application of these methods to the unidentified faults in East Kolaka has high potential for understanding their behavior.

The idea behind this research stems from the occurrence of four significant earthquakes in East Kolaka, Indonesia, during early 2025. The first event, on January 24, 2025, had a moment magnitude (Mw) of 4.9. This was followed by three additional events on January 29, 2025, with moment magnitudes of 5.1, 4.3, and 4.7, respectively. In assessing the regional seismicity, initial analysis of the earthquake epicenters indicates that their locations fall outside the mapped zones of the Middle Kolaka, North Kolaka, and Pelosika faults (PuSGeN, 2024; Soehaimi et al., 2022; Simandjuntak et al., 1993; Surono & Bachri, 2002; Surono, 2010, 2013; Natawidjaja,

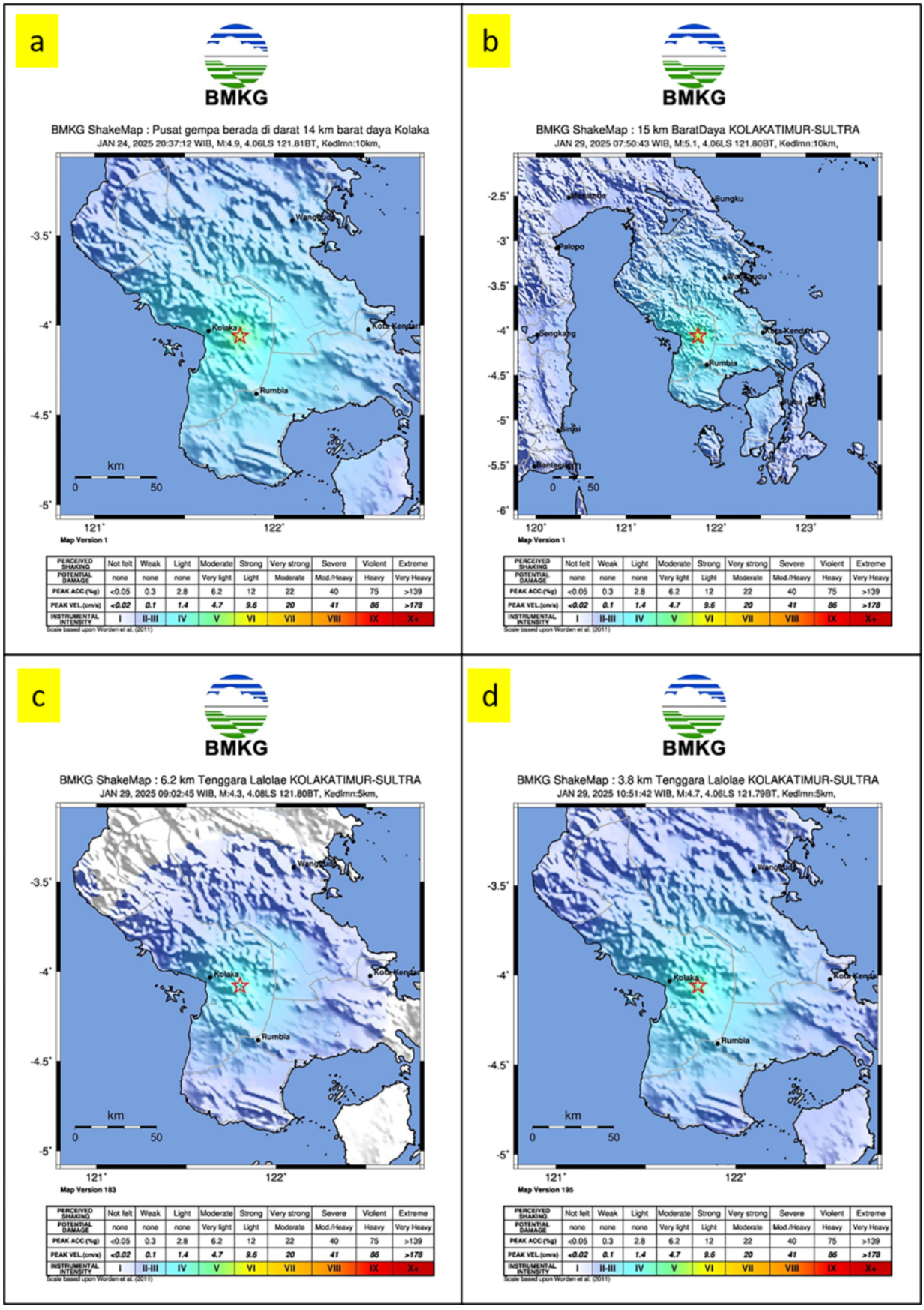

PERCEIVED SHAKING	Not felt	Weak	Light	Moderate	Strong	Very strong	Severe	Violent	Extreme
POTENTIAL DAMAGE	none	none	none	Very light	Light	Moderate	Mod./Heavy	Heavy	Very Heavy
PEAK ACC.(%g)	<0.05	0.3	2.8	6.2	12	22	40	75	>139
PEAK VEL.(cm/s)	*<0.02*	*0.1*	*1.4*	*4.7*	*9.6*	*20*	*41*	*86*	*>178*
INSTRUMENTAL INTENSITY	I	II-III	IV	V	VI	VII	VIII	IX	X+

Scale based upon Worden et al. (2011)

Fig. 1a-d*. Shakemap of the epicenter of East Kolaka earthquake (BMKG, 2025).*

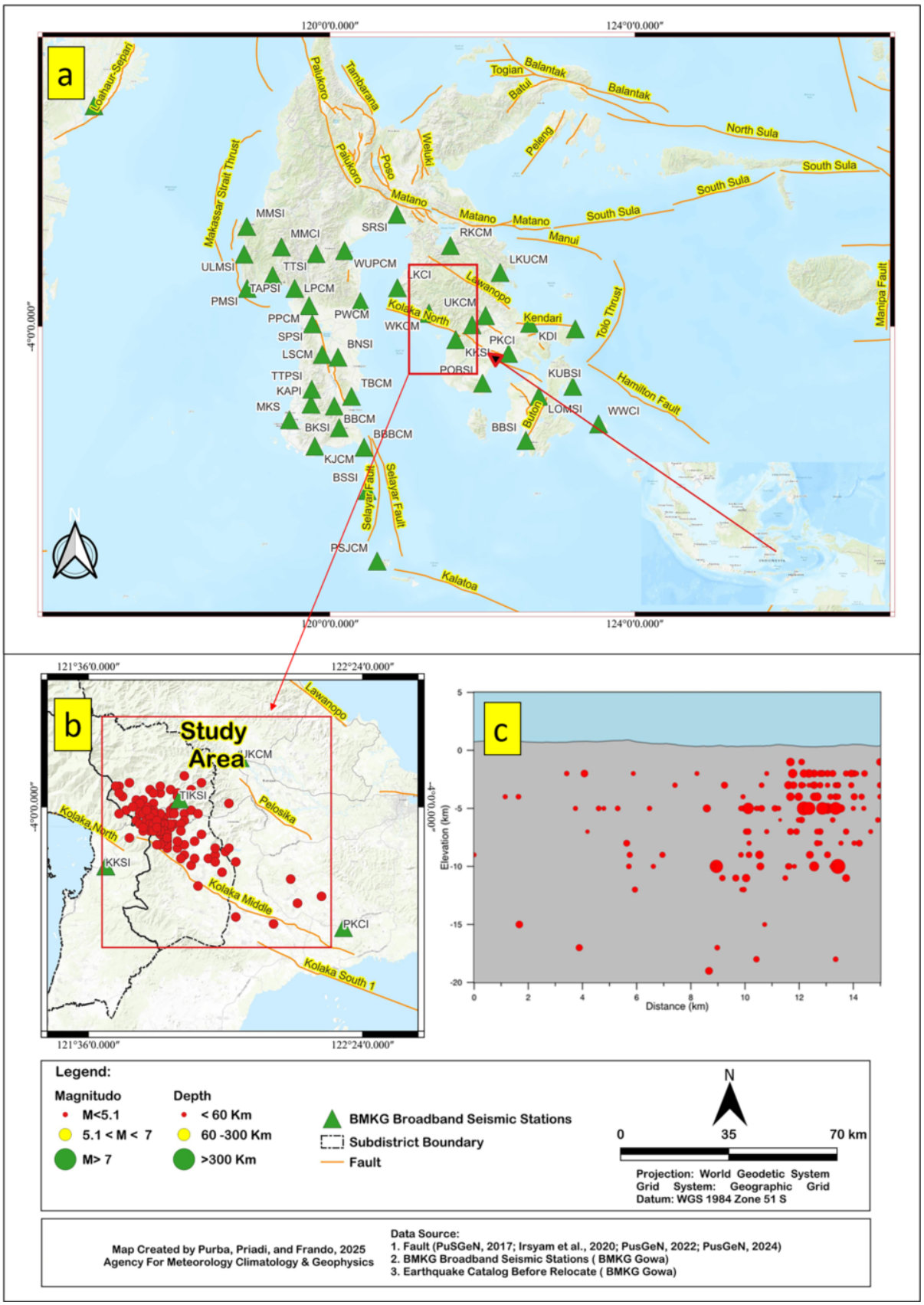

Fig. 2. a) *Map of active fault and BMKG Broadband Seismic Stations around Sulawesi Island,* ***b)*** *study locations in East Kolaka and the earthquake event before relocate (233 events),* ***c)*** *Earthquake depth before relocate.*

2021; Serhalawan & Chen, 2024; Watkinson & Hall, 2017; White et al., 2014). This spatial separation suggests that the January 2025 events may be related to a previously unmapped fault structure (Fig. 2b,c). The observed clustering of seismicity deviates from the known alignments of the Kolaka Fault system, indicating the likelihood of an unidentified fault segment within the study region.

Given this anomaly, this study aims to investigate the possibility of a previously unmapped fault in the region, hereafter referred to as the Purpri Fault, and to characterize its potential structural and seismotectonic features. The primary objective is to assess its structural and seismotectonic characteristics. To achieve this, an integrated geophysical approach is required, incorporating HypoDD for precise earthquake relocation (Waldhauser & Ellsworth, 2000; Waldhauser, 2001; Supendi et al., 2019, 2020, 2022, 2023) and DInSAR for ground deformation analysis (Hanssen, 2001; Hanssen, 2002; Carboni et al., 2022; Fang et al., 2019; Purba et al., 2024a). These methods will collectively help establish the spatial extent, geometry, and seismic potential of the Purpri Fault.

The HypoDD method plays a significant role in making earthquake location more accurate by measuring the differences in seismic wave travel times. This method has been widely applied to refine earthquake catalogs and to delineate seismicity patterns that provide insight into possible fault orientations (Waldhauser & Ellsworth, 2000; Waldhauser, 2001; Supendi et al., 2019, 2020, 2022, 2023). The application of HypoDD to the relocation of seismicity has been confirmed in a number of seismic zones such as the New Madrid Seismic Zone (Dunn et al., 2010; Zhang et al., 2022) and the 2009 L'Aquila earthquake (Di Luccio et al., 2010). In Indonesia, HypoDD has been used efficiently in linking events such as the 2021 Tehoru earthquake (Daniarsyad et al., 2023), the 2021 Flores earthquake (Supendi et al., 2022), and the 2022 Pasaman Earthquake (Supendi et al., 2023) to hitherto unseen fault structures. These studies underscore the method's capacity to map fault systems with high accuracy, which in turn makes it a useful technique for analyzing the Purpri Fault.

DInSAR, a remote sensing technique, has been widely used to detect ground deformation associated with seismic activity. By analyzing surface displacement over time, DInSAR offers an important perspective on fault movement and strain accumulation (ESA, 2012; Fang et al., 2019; Purba et al., 2024a). The use of Sentinel-1 satellite data with DInSAR has proven effective in identifying surface deformation associated with faults in various geological settings, as demonstrated in studies of seismic events in Beijing (Hu et al., 2019), Thessaly (Tolomei et al., 2021), and Kalaotoa (Purba et al., 2024a). These applications illustrate how DInSAR can improve fault mapping and provide insights into the deformation processes associated with active faults such as the Purpri Fault.

Seismic studies in the East Kolaka region have primarily focused on well-established fault segments, including the Middle Kolaka, North Kolaka, and Pelosika faults. The Middle Kolaka and North Kolaka faults exhibit a left-lateral strike-slip mechanism, whereas the Pelosika Fault is characterized a right-lateral strike-slip mechanism (PuSGeN, 2024; Soehaimi et al., 2022; Simandjuntak et al., 1993; Surono, 2010, 2013; Serhalawan & Chen, 2024; Watkinson & Hall, 2017; White et al., 2014). However, recent observations following the January 24, 2025, earthquake sequence suggest that seismicity in the region does not align with these fault systems. The clustering of aftershocks and their spatial distribution (figure 2b–c) indicate the presence of a previously unmapped fault, suggesting a more complex tectonic setting than previously understood. Despite the importance of these findings, current seismic hazard maps by PuSGeN (2024) do not fully incorporate the possibility of additional fault structures in East Kolaka, leaving a significant gap in the understanding of regional fault dynamics.

Although HypoDD and DInSAR have individually been proven effective for fault identification, their integration remains underutilized–particularly in regions like East Kolaka, where fault traces are poorly defined in current seismic hazard models. Given the lack of surface fault mapping and the limitations of each method in isolation, their combined application provides a complementary approach to investigate previously unrecognized fault structures. This study aims to demonstrate the effectiveness of this integrated approach through the case of the newly detected Purpri Fault.

This study aims to identify where this fault is located, assess its structural properties, and evaluate its potential seismic hazard. The occurrence of four earthquakes in early 2025, which do not correspond to the previously mapped Kolaka Fault system, suggests the presence of an unmapped fault. Using an integrated geophysical approach-including HypoDD for seismic relocation and DInSAR to detect surface deformation-this study seeks to provide a comprehensive understanding of the fault's characteristics, its relationship to regional tectonic structure, and its implications for seismic risk assessment.

The novelty of this study lies in the discovery and investigation of unmapped active faults in East Kolaka. While previous studies have focused on the Central Kolaka, North Kolaka and Pelosika faults (PuSGeN, 2024; Soehaimi et al., 2022; Simandjuntak et al., 1993; Surono, 2010, 2013; Serhalawan & Chen, 2024; Watkinson & Hall, 2017; White et al., 2014), this study introduces new evidence suggesting that seismic activity in the region is not only caused by known fault systems. The integration of advanced geophysical methods enables a more detailed analysis of fault segmentation and interaction, providing insight into the complex tectonic dynamics of the area. This research not only contributes to the scientific understanding of fault mechanics in Southeast Sulawesi, but also provides important data for updating seismic hazard models and disaster mitigation strategies.

Data and Method

Hypocenter Double-Difference (HypoDD)

To accurately determine the locations of the mainshock and aftershocks in East Kolaka, this study employs the double-difference (DD) method, implemented through the HypoDD algorithm. This approach, developed by Waldhauser & Ellsworth (2000) and refined by Waldhauser (2001), enhances earthquake relocation accuracy by minimizing errors in seismic travel time calculations. The method is based on the assumption that closely spaced earthquake pairs share similar ray paths and travel times when observed from distant stations. By analyzing the differences in arrival times between pairs of earthquakes recorded at the same station, this method effectively reduces location uncertainties caused by velocity model variations, producing a clearer image of fault structures and seismic clustering.

The earthquake data used in this study were obtained from the BMKG Geophysical Station Gowa (Indonesian Meteorological, Climatological, and Geophysical Agency) catalogue, covering the period from January 24, 2025, to February 7, 2025. These data were extracted from continuous recordings by broadband seismic stations, represented by green triangles in Fig. 2 a. A total of 233 events, with magnitudes ranging from 1.2 to 5.1, were identified from mainshocks and aftershocks (Fig. 2b, c). Initial hypocenter locations were determined using the LocSAT (Bratt & Nagy, 1991) linearized inversion routine, integrated into the SeisComP4 program (Hanka et al., 2010). This process relied on the IASP91 velocity model (Kennett & Engdahl, 1991; Kennett et al., 1995) as a reference for the initial earthquake locations.

To improve the accuracy of these preliminary locations, we applied the double-difference method to relocate the earthquakes. In this method, the travel time residual between observed and calculated travel times for an earthquake pair is expressed as (Waldhauser, 2001 Waldhauser & Ellsworth, 2000; Waldhauser & Schaff, 2007):

$$d_k^{ij} = \left(t_k^i - t_k^j\right)^{obs} - \left(t_k^i - t_k^j\right)^{cal} \quad (1)$$

Where:

t_k^i and t_k^j represent the travel times of seismic waves from earthquakes and to station , respectively.

For this study, event pairs were selected based on P- and S-wave travel time similarities, ensuring that only closely related seismic events were included in the relocation process. The maximum hypocentral separation was set to 200 km, with up to 30 neighboring earthquakes per event. A minimum of 5 links was required to define a neighboring pair, and the maximum distance between the cluster centroid and a seismic station was set at 200 km. These parameter choices were extensively tested to achieve an optimal balance between computational efficiency and relocation accuracy.

Travel times were recalculated using this velocity model and compared with observed arrival times at seismic stations. The relocation process iteratively adjusted earthquake positions to minimize the residuals between theoretical and observed travel times, significantly improving the accuracy of the fault structure delineation.

To assess the reliability of the relocated earthquake positions, a bootstrap resampling method (Billings, 1994) was applied. This statistical technique introduced Gaussian noise with a standard deviation of 0.1 seconds to simulate realistic observational uncertainties. The relocation process was repeated 5 times, generating small perturbations in the hypocenter locations for each event. From these perturbations, 95% confidence ellipsoids were calculated, providing a quantitative measure of the uncertainty in the relocated positions. This assessment ensured that the final earthquake locations provided the most accurate representation of the Purpri Fault's seismic activity, offering a clearer understanding of its structure and potential seismic hazards.

Differential Interferometric Synthetic Aperture Radar (DInSAR)

The Differential Interferometric Synthetic Aperture Radar (DInSAR) method was employed in this study to detect ground displacement associated with fault activity. DInSAR utilizes Synthetic Aperture Radar (SAR) images taken at different times to measure phase differences in radar waves, which correspond to surface deformation (Ferretti et al., 2007a). These phase differences are processed to generate interferograms, which provide a visual representation of ground movement (Ferretti et al., 2007b). The total phase difference between two SAR images in an interferogram can be expressed as (Hansen, 2001, 2002; Rocca et al., 2007c):

$$\Delta\varphi = \Delta\varphi_{flat} + \Delta\varphi_{elevation} + \Delta\varphi_{deformation} + \Delta\varphi_{atmosfer} + \Delta\varphi_{noise}$$

Where:

$\Delta\varphi flat$ represents the phase difference due to topographic effects, $\Delta\varphi elevation$ accounts for phase changes caused by elevation variations, and $\Delta\varphi deformation$ corresponds to ground displacement. Additionally, $\Delta\varphi atmosfer$ represents phase shifts caused by atmospheric disturbances, while $\Delta\varphi noise$ includes errors from measurement uncertainties. Each component influences the interferometric phase, and by isolating these effects, DInSAR enables precise measurement of surface deformation (Manzo et al., 2011; Arangio et al., 2013; Luebeck et al., 2020).

The SAR data used in this study were acquired from the Sentinel-1A satellite for the period January 8, 2025 – February 1, 2025, and downloaded from the Alaska Satellite Facility (ASF) archive (https://search.asf.alaska.edu) (Table 1). The Sentinel-1 dataset consists of two master-slave image pairs, ensuring broader coverage of the study area. The master image from January 8, 2025, served as the reference, while the slave image from February 1, 2025, was used as the secondary observation. This approach allowed the generation of interferograms that capture surface deformation during this period.

Table 1. *The Sentinel 1 data used.*

No.	Acquisition Date	Level	Acquisition	Polarization	Viewpoint
1.	08 January 2025	1.0	IW	VV	Descending
2.	08 January 2025	1.0	IW	VV	Descending
3.	01 February 2025	1.0	IW	VV	Descending
4.	01 February 2025	1.0	IW	VV	Descending

Notes:
The four SLC data used in this research are:
a. S1A_IW_SLC__1SDV_20250108T213527_20250108T213554_057358_070F29_1808
b. S1A_IW_SLC__1SDV_20250108T213552_20250108T213620_057358_070F29_BB60
c. S1A_IW_SLC__1SDV_20250201T213525_20250201T213552_057708_071D04_5D51
d. S1A_IW_SLC__1SDV_20250201T213550_20250201T213618_057708_071D04_C6FA

Given the extensive study area, a single interferogram was insufficient to capture the entire region's deformation. Therefore, four SAR images were used, forming two interferogram pairs to increase the spatial coverage. The first two images were combined to produce one image as well as the second image. The results of the merging were then combined to produce an interferogram. This merging ensures that all relevant deformation signals within the study area are accounted for. Interferogram processing was conducted using the Sentinel Application Platform (SNAP) version 9.0.0, an open-source software developed by the European Space Agency (ESA, 2012).

The workflow involved several key steps: (1) The process began with TOPSAR Split, which was used to isolate the relevant bursts and sub-swaths from the Sentinel-1A dataset, focusing on the area cover-

ing the Purpri Fault (Clerici et al., 2017), (2) Next, Apply Orbit File was employed to insert precise orbital data, correcting for satellite position and velocity to ensure geometric accuracy (Mancini et al., 2021; Lee et al., 2025), (3) Radiometric calibration and speckle noise filtering were then applied to enhance the clarity of radar backscatter and improve the signal-to-noise ratio, (4) The co-registration process was conducted through Back Geocoding, aligning the master and slave images using the SRTM 1 arc-second (30 m) DEM and orbital parameters to preserve phase coherence (Richards, 2009), (5) To further improve image alignment and coherence across burst overlaps, Enhanced Spectral Diversity (ESD) was applied (Fang et al., 2023), (6) The interferogram was then formed by calculating phase differences between the co-registered master and slave images, capturing surface displacement along the satellite's line of sight (Ferretti et al., 2007b), (7) All bursts were merged using TOPSAR Deburst to create a seamless interferometric image, (8) Topographic Phase Removal was carried out using the same SRTM DEM to eliminate the elevation-induced phase component and isolate the deformation signal (Zebker & Goldstein, 1986; Hanssen, 2001), (9) The result was then subjected to Multilooking, which resampled the data to square pixels and reduced high-frequency speckle noise (Xu et al., 2022), (10) To enhance the unwrapping process, Goldstein Phase Filtering was applied, which effectively suppressed noise while retaining the phase signal (Goldstein & Werner, 1998), (11) The filtered interferogram was exported using SNAPHU Export, allowing phase unwrapping to be performed externally with the SNAPHU algorithm, which resolves phase ambiguity through a minimum-cost flow approach (Chen & Zebker, 2002), (12) Once unwrapped, the final deformation map was geocoded using Range-Doppler Terrain Correction to project the radar coordinates into geographic coordinates (Meyer & Sahr, 2004; Zhang et al., 2012; Nedelcu & Brisco, 2018). This processing workflow was carried out following best practices from previous studies (McGarragh et al., 2015; Clerici et al., 2017; Markogiannaki et al., 2020; Carboni et al., 2022; Purba et al., 2024a), ensuring high-quality and reliable results. By integrating these processing techniques, this study effec-tively analyzed ground deformation related to fault activity, providing valuable insights into the movement of the newly identified Purpri Fault.

Results

Historical Seismicity Analysis (2015–2024)

To assess whether the 2025 earthquake sequence represents an isolated swarm or part of a broader long-term tectonic pattern, we examined historical seismicity in the Kolaka region from 2015 to 2024 using the catalogue from BMKG Geophysical Station Gowa (Indonesian Meteorological, Climatological, and Geophysical Agency). The analysis reveals that historical seismicity in the broader Kolaka region has been largely concentrated along the Kendari Fault (Fig. 3), particularly in the Kendari North & Central segment, likely influenced by compressional forces from the Tolo Thrust (Hall, 2019; Serhalawan & Chen, 2024). In contrast, seismic activity along the Kolaka Fault system–which comprises the North, Middle, and South segments–has shown more variable behavior. The Kolaka North Fault has a documented history of damaging earthquakes, including a significant event in 2011 (BMKG, 2019; Pasari et al., 2021). However, the Kolaka Middle segment, which lies closest to the 2025 earthquake sequence, shows no record of major or damaging historical earthquakes, suggesting relatively low past activity.

The fault systems in Kolaka have been interpreted through both geophysical (e.g., Serhalawan & Chen, 2024; PuSGeN, 2024) and geological (e.g., Soehaimi et al., 2022; Simandjuntak et al., 1993; Surono, 2010, 2013; White et al., 2014; Watkinson & Hall, 2017) perspectives, the Kolaka Middle segment is interpreted as a left-lateral strike-slip fault, inferred from its structural orientation and deformation trends. The 2025 earthquake sequence, however, presents a contrasting oblique-normal faulting mechanism, as observed in both the foreshock and mainshock focal mechanisms, with significant vertical motion inconsistent with a pure strike-slip regime. This kinematic discrepancy suggests that the 2025 sequence may not be associated with typical Kolaka Middle behavior.

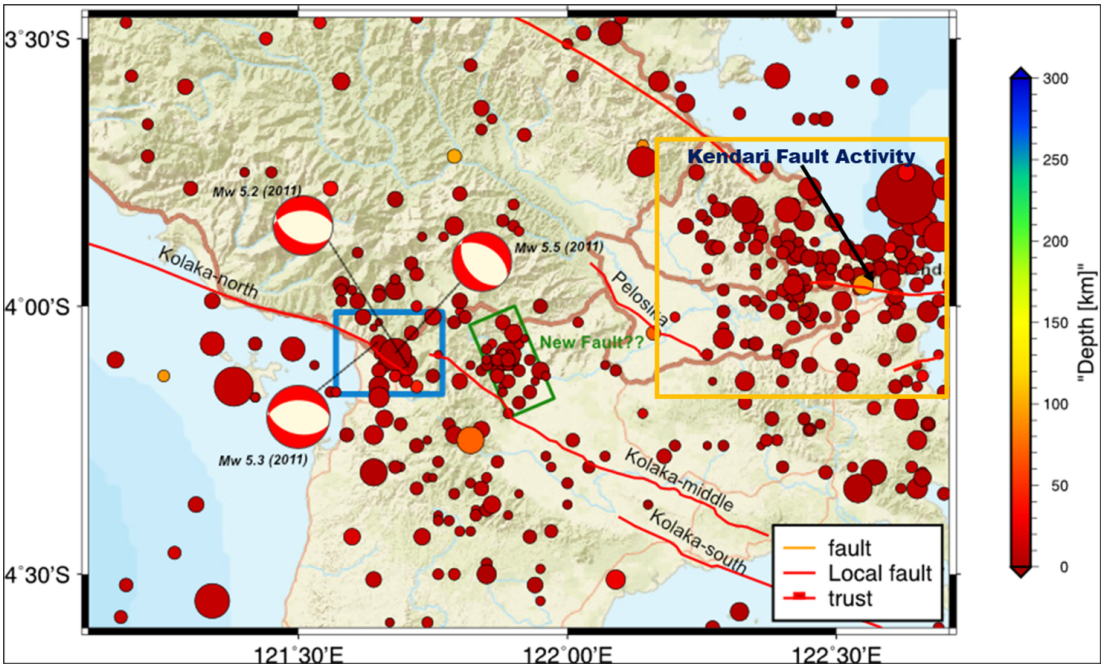

Fig. 3. *Historical seismicity from 2015 to 2024 showing dominant activity along the Kendari Fault and minimal events in the area surrounding the inferred Purpri Fault.*

One possibility is that this earthquake cluster reveals deformation occurring along an unmapped fault segment or a structural discontinuity between known segments. While oblique or reverse-slip components can emerge along strike-slip faults under localized compression, the spatial pattern, rupture orientation (southeast–northwest), and hypocenter distribution of the 2025 events differ significantly from the mapped Kolaka trace. The mainshock occurred in the central cluster, located east of and offset from the Kolaka Middle segment. This strengthens the hypothesis that the sequence may be associated with a previously unrecognized fault.

Comparisons with the Pelosika Fault, located further southeast, support this interpretation. Although the Pelosika Fault is known to exhibit shallow to intermediate-depth seismicity (5–60 km), it has generally low-to-moderate activity (M2–M4) and lacks a clear history of large events near its mapped trace. Similarly, the Kolaka Middle segment shows sparse historical activity. This raises doubts about either of these structures being the primary source of the 2025 earthquakes, especially considering the clear difference in fault kinematics.

Earthquake Relocation of the Mainshock

The relocation of seismic events from January 24 to February 7, 2025, using the HypoDD algorithm as seen on Fig. 4a (Waldhauser & Ellsworth, 2000; Waldhauser, 2001; Waldhauser & Schaff, 2007), initially focused on the mainshock (Mw 5.1) that occurred on January 29, 2025. This event was recorded at a depth of 10 km and exhibited an oblique-normal focal mechanism, with a strike of 142°, dip of 48°, and rake of –83° based on moment tensor inversion (Heimann, 2011). These parameters indicate dominant normal faulting with a minimal horizontal slip.

The preliminary relocation map did not yet reveal clear clustering or a fault-aligned distribution, as it included only the mainshock and limited foreshocks. However, it suggested a southeastward dipping fault geometry. This initial result served as the basis for more comprehensive relocation of the full aftershock sequence.

A dashed green line was added to represent the estimated surface trace of the fault based on the mainshock alignment. The shallow depth and

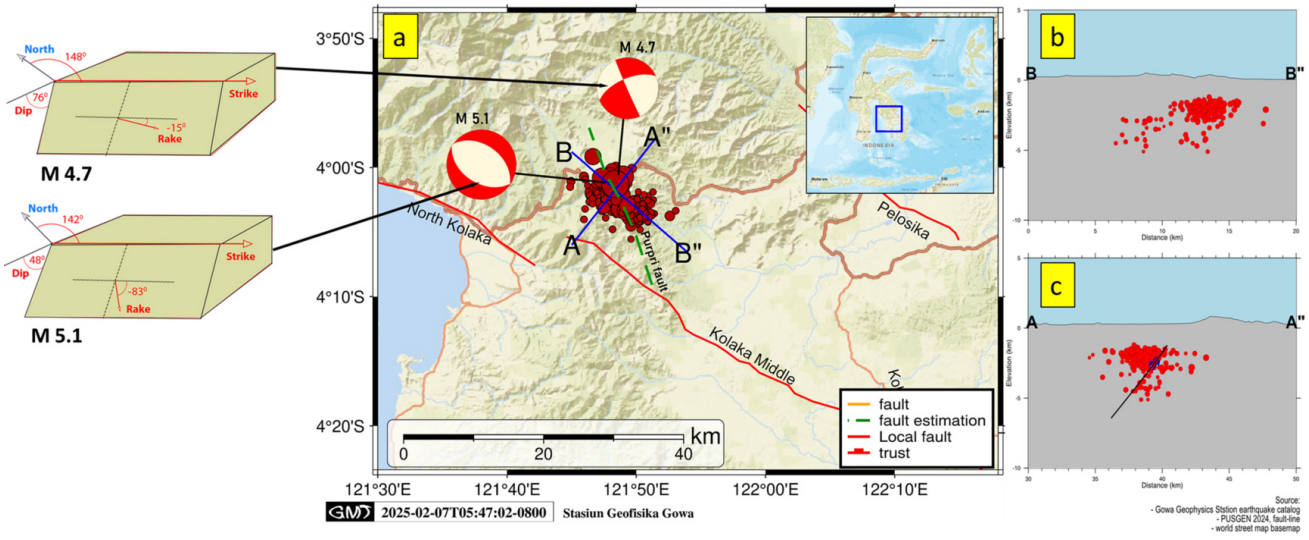

Fig. 4. a) *Relocated epicenters of the M 5.1 mainshock and after shock with focal mechanism illustration;* ***b)*** *Cross-sectional profile B-B';* ***c)*** *Cross-sectional profile A-A'.*

oblique-normal kinematics suggest that this fault is capable of generating damaging ground motion, meriting further structural interpretation through the full sequence analysis. Cross-sectional profiles (Fig. 4b, c) along transects A–A′ and B–B′ further confirm a steeply dipping fault geometry with hypocenters predominantly confined to the upper 10 km of the crust, consistent with shallow seismogenic activity capable of producing damaging ground shaking.

Spatiotemporal Clustering of the 2025 Sequence

To better understand the structural organization of the 2025 seismic sequence, we conducted a comprehensive relocation of 233 events recorded between January 24 and February 7, 2025. The results revealed a clear spatiotemporal clustering of hypocenters into three distinct groups: a northern cluster, a central cluster (hosting the mainshock), and a southern cluster. These clusters are aligned along a southeast–northwest trend, which is oblique and offset from the mapped trace of the Kolaka Middle Fault, indicating structural independence. In Figure 5, black dots represent the original epicenter locations prior to relocation, while green dots denote the relocated hypocenters using the HypoDD method. The comparison clearly illustrates how the relocation process significantly improves the spatial resolution of the dataset. Initially, the events appeared diffusely scattered, lacking any apparent structural pattern. After relocation, however, the events align into three distinct clusters–northern, central, and southern–along a southeast–northwest orientation. This refinement reveals a coherent fault structure that was not evident in the unrelocated data and provides further support for the delineation of the Purpri Fault.

The central cluster corresponds spatially to the strongest DInSAR deformation, reinforcing its association with the inferred Purpri Fault. The presence

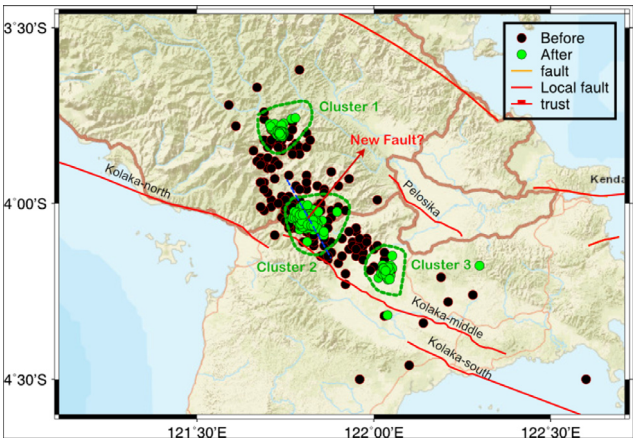

Fig. 5. *Spatiotemporal Clustering of the 2025 Sequence.*

of systematic clustering in both space and focal depth provides evidence for segmented fault activity, rather than random aftershock dispersion.

The relocation results exhibit low RMS residual values (Fig. 6), with most events having residuals close to zero, indicating strong convergence and reliable location accuracy. Nevertheless, the relocation process was constrained by the limited number of seismic stations in the region. Due to the small magnitudes (Mw 1–2) of many aftershocks, some events were recorded by only three or four stations, introducing increased uncertainty. Despite this limitation, the overall clustering pattern and consistency in focal mechanisms support the interpretation of a previously unmapped, segmented fault system.

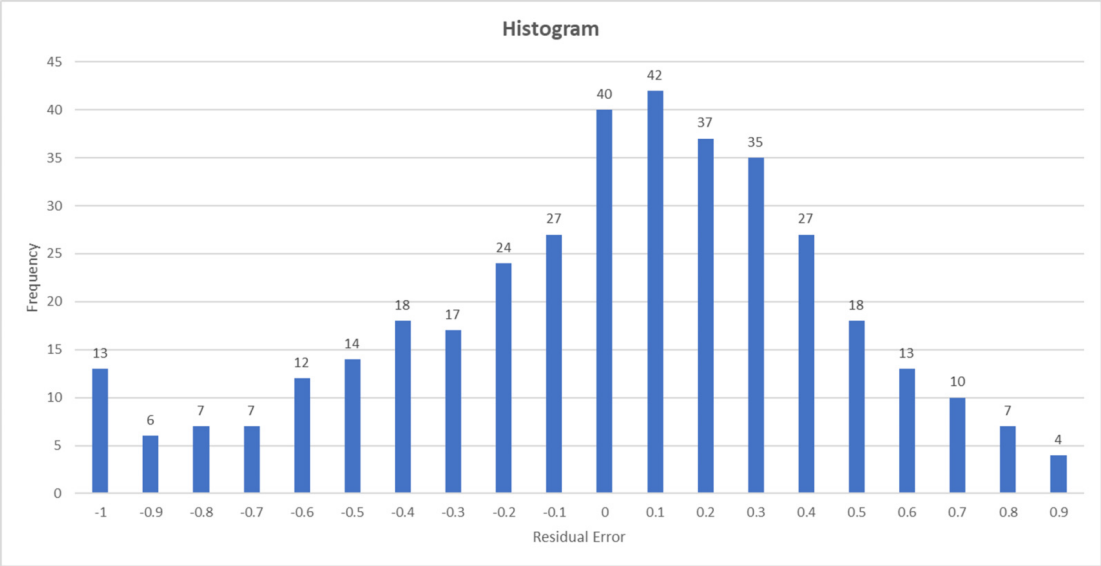

***Fig. 6**. Histogram of relocation residual error.*

The focal mechanism results in this study support the interpretation of oblique-normal faulting along the Purpri Fault. However, we recognize that there are uncertainties in these results, especially because the number of seismic stations in the study area is limited. As highlighted by Purba et al. (2025b), the accuracy of focal mechanism solutions depends heavily on how well the stations are distributed and how precisely wave polarities can be observed. In our dataset, some events were recorded by only 3 to 4 stations, which may reduce the accuracy of the calculated strike, dip, and rake values. Even so, the similarity of focal mechanisms among clustered events, and their consistency with the surface deformation pattern, gives us confidence that the faulting style we interpret is reliable. While the focal mechanism solutions in this study provide key evidence for oblique-normal faulting along the Purpri Fault, we acknowledge that uncertainties are inherent in such analyses, particularly given the limitations of station coverage in the region.

Ground Deformation from DInSAR Analysis

The DInSAR results, derived from Sentinel-1A SAR imagery spanning January 8 to February 1, 2025, reveal clear evidence of ground deformation along the Purpri Fault. The interferograms (Fig. 7) show distinct patterns of subsidence and uplift, corresponding well with the relocated hypocenters (Figs. 4a & 5). The deformation analysis indicates that the western block of the fault has subsided by approximately -13 cm, while the eastern block has uplifted by around +11 cm. This asymmetric displacement pattern is consistent with the oblique-normal faulting mechanism derived from the focal mechanism solution, further confirming the fault's role in controlling crustal deformation in the region.

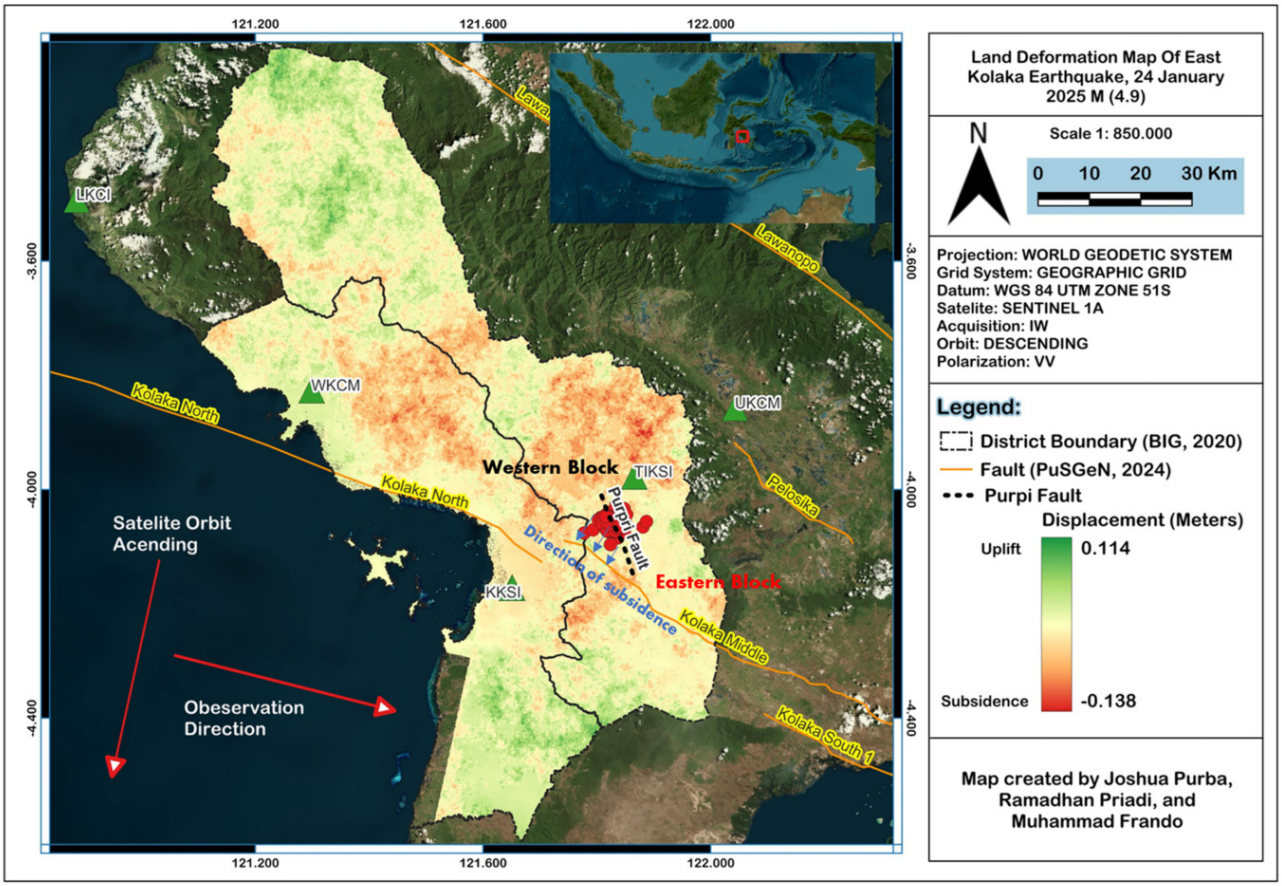

Fig. 7. *Deformation map in the East Kolaka.*

The Sentinel-1A data were acquired in ascending orbit, with the satellite moving from southwest to northeast and observing the Earth's surface from the west. This right-looking geometry produces line-of-sight (LOS) deformation measurements that are sensitive to both vertical and east–west horizontal displacements. In this configuration, uplift and/or eastward motion appears as positive LOS displacement (green), while subsidence and/or westward motion appears as negative displacement (red). The deformation pattern observed—uplift of the eastern block and subsidence of the western block—is therefore interpreted as primarily vertical motion along an oblique-normal fault plane.

Profiles extracted from DInSAR-derived deformation maps (Fig. 7) along the fault trace (dashed black line) also show differential vertical movement, reinforcing the interpretation that the Purpri Fault is actively accommodating strain release through a combination of normal and left-lateral slip.

Discussion

The results of this study confirm that the Purpri Fault is a newly identified active fault in East Kolaka, clearly distinct from the Middle Kolaka and North Kolaka Faults, which are predominantly characterized by left-lateral strike-slip motion (Simandjuntak et al., 1993; Surono, 2010, 2013; White et al., 2014; Watkinson & Hall, 2017; Soehaimi et al., 2022; Serhalawan & Chen, 2024; PuSGeN, 2024). Evidence from relocated hypocenters, focal mechanism solutions, and ground deformation patterns obtained from DInSAR analysis consistently indicates that the Purpri Fault exhibits an oblique-normal faulting mechanism, with significant normal displacement coupled with a left-lateral shear component. These results are broadly consistent with the preliminary findings of Wijayanto et al. (2025), who also noted the presence of an unmapped fault in East Kolaka based only on seismic relocation data.

The distribution of earthquake depths suggests that the Purpri Fault accommodates shallow crustal deformation, with most seismic events occurring at depths less than 10 km. This shallow depth of rupture enhances the likelihood of strong ground shaking, raising concerns regarding its potential impact on infrastructure and human settlements (Sreejith et al., 2016; Craig, 2019; Minson et al., 2020). Furthermore, the clustering of seismicity along linear, well-defined patterns implies structural segmentation within the fault zone, which may play a critical role in controlling rupture initiation and propagation during future earthquakes (Delogkos et al., 2020; Wu et al., 2020; Natawidjaja et al., 2021).

This newly emerged clustering behavior not only reinforces the presence of the Purpri Fault but also suggests structural segmentation along its length, which could influence rupture dynamics and seismic hazard potential in future events.

Long-term seismicity analysis from 2015 to 2024 confirms that the region surrounding the Purpri Fault was largely aseismic prior to the 2025 sequence, with most recorded events concentrated along the Kendari Fault and no significant activity associated with the Kolaka Middle segment. This quiescence strengthens the interpretation that the 2025 sequence represents a new activation episode rather than continued behavior along a previously active fault. The initial relocation of the mainshock and its foreshocks revealed a southeast-dipping fault plane, but lacked a broader structural context. However, the full sequence relocation uncovered a distinct three-cluster pattern—northern, central, and southern—aligned southeast–northwest and offset from the Kolaka Fault trace. This clustering pattern, confirmed by low RMS values, indicates segmented rupture behavior and provides further evidence for a previously unmapped, structurally coherent fault zone.

The correlation between seismic and geodetic data provides compelling evidence of the fault's activity. The spatial alignment between relocated hypocenters and DInSAR-derived deformation–characterized by subsidence on the western block and uplift on the eastern block–indicates that the Purpri Fault is actively accommodating tectonic strain. This deformation pattern supports the interpretation that strain is released through both seismic rupture and aseismic slip processes (Fang et al., 2019; Markogiannaki et al., 2020; Carboni et al., 2022).

Despite the strong spatial correlation between the relocated seismicity and DInSAR-derived deformation, it is essential to acknowledge a key limitation of the DInSAR technique: its sensitivity is restricted to displacements occurring along the satellite's Line-of-Sight (LOS). In the case of Sentinel-1A's ascending orbit, the LOS vector is primarily sensitive to vertical and east–west ground motion components. However, this configuration inherently limits the ability to distinguish vertical uplift/subsidence from horizontal motion, particularly in the north–south direction, which is orthogonal to the LOS (Manzo et al., 2011; Atzori & Antonioli, 2011; Wang et al., 2019). As such, the inferred oblique-normal faulting mechanism–while supported by the deformation pattern–remains partially constrained due to the one-dimensional nature of the LOS measurement. Without complementary observations, such as descending-orbit SAR acquisitions, GNSS data, or 3D InSAR decomposition, the full kinematic interpretation of the fault movement cannot be conclusively established (Hu et al., 2010; Castaldo et al., 2017). Future research integrating these datasets will be essential to resolve the three-dimensional deformation field and validate the inferred fault geometry with greater certainty.

By combining two independent but complementary geophysical approaches–earthquake relocation using HypoDD and deformation mapping using DInSAR–this study achieves a comprehensive validation of the Purpri Fault as an active tectonic structure. This integration is particularly valuable in regions where surface fault traces are poorly developed or concealed by surface conditions. The methodology underscores the importance of multi-multidiscipline approaches for fault identification, as has been demonstrated in numerous regional and international case studies.

The discovery of the Purpri Fault has significant implications for seismic hazard assessment in Southeast Sulawesi. Currently, this fault is not incorporated into official regional hazard models, such as those published by PuSGeN (2024), which may re-

sult in an underestimation of earthquake risk in the area. Based on its shallow depth, oblique-normal kinematic behavior, and the surface deformation observed through DInSAR, the Purpri Fault presents a credible threat of generating damaging earthquakes. To estimate its potential seismic capacity, we apply the empirical relationship by Wells & Coppersmith (1994), which relates surface rupture length to maximum expected magnitude. Given the fault's inferred trace length of approximately 17 km, the estimated maximum moment magnitude is ~6.5. While this value is theoretical and subject to geological confirmation.

The geological context of the Purpri Fault further supports these findings. The fault is situated within the Mekongga Complex, composed primarily of metamorphic units such as schist, gneiss, and quartzite (Simandjuntak et al, 1993; Surono, 2010, 2013; White et al., 2014; Hasrul et al., 2021; Serhalawan & Chen, 2024). These lithologies exhibit markedly different mechanical responses to tectonic loading. Schist, with its prominent foliation due to aligned mica minerals, is highly anisotropic and more susceptible to shear and differential strain, especially near the surface (White et al., 2014; Hasrul et al., 2021). This behavior is attributed to the orientation of platy minerals such as biotite and muscovite along foliation planes, which facilitate shear localization and strain accumulation under tectonic stress (Stallard & Shelley, 2005; Huesca-Pérez et al., 2016; Mamot et al., 2020). Studies have shown that shear wave velocities vary significantly when propagating parallel versus perpendicular to schistosity, highlighting the inherent mechanical anisotropy of schist (Huesca-Pérez et al., 2016).

Gneiss, though generally stronger and less foliated than schist, can also exhibit localized deformation due to its compositional banding (Hasrul et al., 2021). The presence of alternating felsic and mafic layers can result in stress concentration and partial strain accommodation under compressional or extensional regimes (Mamot et al., 2020; Waqas et al., 2024). For instance, Oliva-Urcía et al. (2012) emphasize that the alignment of feldspar and mica grains within gneissic fabrics influences its overall rheological behavior, allowing strain to localize in specific zones without the pervasive foliation typical of schist.

In contrast, quartzite behaves as a massive and brittle lithology with minimal foliation, resulting in a relatively isotropic and highly competent mechanical response (Hasrul et al., 2021). Its deformation resistance is primarily due to the interlocking nature of quartz grains and the lack of preferred mineral orientation, which limits its susceptibility to strain concentration or shear displacement (Roselli et al., 2010; Adam et al., 2020; Waqas et al., 2024). Consequently, quartzite is more likely to fracture than to deform plastically, acting as a rigid tectonic block during faulting.

Based on the vertical deformation pattern observed in DInSAR, it is inferred that the western subsiding block of the Purpri Fault is dominated by schist, which accommodates vertical strain more readily. In contrast, the eastern uplifting block likely comprises gneiss or quartzite, whose greater mechanical strength leads to more distributed or rigid responses to tectonic loading. This lithological asymmetry provides a plausible explanation for the contrasting deformation behavior across the fault trace.

Although the spatial and kinematic evidence supports the interpretation of the Purpri Fault as a previously unmapped active structure, we acknowledge that other tectonic or hydromechanical processes may have contributed to the observed seismicity. One possible mechanism is stress transfer from nearby fault systems, such as the Kolaka north/middle, which may have experienced recent aseismic slip or coseismic stress changes capable of perturbing stress fields in the surrounding crust (Barros et al., 2019; Danré et al., 2024).

Another plausible explanation involves secondary faulting, where shallow slip occurs along pre-existing zones of weakness rather than primary mapped structures. Such behavior has been observed in other tectonic settings, including the 2016 Kumamoto Earthquake (Fukushima & Ishimura, 2020), and underscores the complexity of fault interactions during strain accumulation and release.

The potential role of fluid-induced seismicity also warrants consideration. Although there is no known anthropogenic fluid injection activity in East Kolaka, the geological setting of the Purpri Fault within the Mekongga Complex suggests conditions that could naturally facilitate fluid migration. In par-

ticular, schist and gneiss exhibit strong foliation and compositional banding, which may act as conduits for deep-seated fluids released during metamorphism. These fluids can locally increase pore pressure, reduce effective normal stress on fault planes, and trigger fault slip (Guglielmi et al., 2008; Kim, 2013; McGarr, 2014). Previous studies have shown that fluid-filled fractures and metamorphic foliation planes in anisotropic rocks can modulate microseismicity and fault creep, especially in the upper crust (Goebel et al., 2016; Yoshida & Hasegawa, 2018).

While our data currently support a tectonic origin for the observed seismicity, acknowledging these alternative mechanisms provides a more comprehensive interpretation. We recommend future geochemical, geomechanical, and hydrogeological investigations to further evaluate the potential influence of fluids and fault interactions in this region.

The mechanical contrast between these lithologies is likely to influence not only the fault geometry but also the distribution of damage during earthquakes. Although the shakemap (Fig. 1) indicates a relatively low to medium peak ground acceleration of approximately 27.4- 60.8gal (equivalent to 2.8%g – 6.2%g, or MMI IV-V), field observations recorded structural damage in many one-story buildings. According to the official report from the Regional Disaster Management Agency (BPBD) of East Kolaka, a total of 159 residential structures were damaged (BPBD, 2025). This suggests that local amplification may have occurred, possibly due to the deformable nature of schist and the shallow rupture depth of the event. Short-period ground motions–characteristic of shallow, moderate-magnitude earthquakes–are especially damaging to low-rise, unreinforced structures, particularly when underlain by materials that amplify seismic waves (Asrurifak, 2010; PuSGeN, 2022; Purba et al., 2024b, 2025a).

To enhance regional seismic hazard assessments, future research should prioritize long-term geodetic monitoring to observe temporal changes in strain accumulation and deformation patterns (Elliott et al., 2010; Xu et al., 2010; Li et al., 2011; Fielding et al., 2013). Both deterministic and probabilistic seismic hazard models need to be updated to reflect the presence and behavior of the Purpri Fault (Pailoplee et al., 2009; Purba et al., 2024b, 2025a). Incorporating this fault into national hazard frameworks will be crucial for strengthening earthquake preparedness and mitigation strategies.

In addition, future studies should aim to deepen our understanding of the seismotectonic characteristics and dynamic behavior of the Purpri Fault. Long-term geodetic datasets from continuous GPS networks and extended InSAR time series will be indispensable for tracking interseismic strain and detecting potential precursory deformation signals (Elliott et al., 2010; Xu et al., 2010; Li et al., 2011; Fielding et al., 2013). While this study employed Sentinel-1 C-band SAR data, the integration of L-band imagery from ALOS PALSAR-2 is recommended due to its enhanced penetration in vegetated and topographically complex terrain, allowing for more accurate and reliable deformation measurements (DE Alban et al., 2018; Liu et al., 2020). The fusion of C-band and L-band data is likely to improve the resolution and stability of surface deformation analysis over time.

The accuracy of hypocenter relocation can be further improved by adopting region-specific seismic velocity models. This study used the IASP91 global 1D model (Kennett & Engdahl, 1991); however, the application of local or 3D velocity models could reduce location uncertainty and refine the geometric representation of fault structures, thereby enhancing seismic hazard quantification. Complementary paleoseismological investigations, including trenching and dating of past rupture events, are also essential to estimate the recurrence intervals of large earthquakes along the Purpri Fault (Daryono, 2016; Howarth et al., 2018; Williams et al., 2019). Furthermore, numerical fault modeling and dynamic rupture simulations could contribute to more realistic earthquake scenario planning (Silva et al., 2020).

In conclusion, this study demonstrates that the Purpri Fault is an active, seismogenic structure with the capacity to generate damaging earthquakes. The integration of seismological and geodetic techniques has proven effective in fault characterization, offering critical insights for hazard mitigation. These findings emphasize the urgent need to revise seismic hazard models, expand geophysical monitoring networks, and develop targeted risk reduction strategies for the East Kolaka region and beyond.

Conclusions

This study presents the identification and characterization of the Purpri Fault, a previously unmapped active fault in East Kolaka, Indonesia. Through the integration of seismic relocation using the HypoDD method and ground deformation analysis from Sentinel-1A DInSAR data, the Purpri Fault is shown to be an independent seismogenic structure, distinct from the established Kolaka Fault system. The fault exhibits an oblique-normal mechanism, accommodating both extensional and left-lateral strike-slip motion, with seismicity predominantly concentrated in the shallow crust (<10 km depth).

DInSAR-derived surface displacement, marked by subsidence on the western block (–13 cm) and uplift on the eastern block (+11 cm), corresponds spatially with the relocated seismicity, reinforcing the interpretation that the fault is actively releasing accumulated strain. The coherence between seismological and geodetic observations confirms the structural and tectonic significance of the Purpri Fault within the regional stress regime.

The recognition of this fault has important implications for seismic hazard assessments in Southeast Sulawesi, as it is currently absent from existing regional fault models. Its shallow seismic activity and capacity for significant surface deformation suggest a high potential for moderate to strong earthquakes, underscoring the need for its incorporation into updated hazard frameworks.

Future investigations should prioritize high-resolution seismic velocity modeling, continuous GPS and InSAR monitoring, paleoseismological trenching, and numerical rupture simulations to refine the fault's kinematics, recurrence intervals, and rupture potential. This study demonstrates the importance of integrating multiple geophysical techniques in fault characterization and emphasizes the need for proactive seismic hazard assessments to enhance earthquake preparedness and disaster risk mitigation strategies in Southeast Sulawesi.

Acknowledgements

The authors would like to thank the Meteorology, Climatology and Geophysics Agency, especially the team from the Gowa Geophysical Station for helping to complete this research. We would like to express our sincere gratitude to the two anonymous reviewers for their valuable comments and constructive suggestions, which have greatly contributed to improving the quality of this paper.

Conflict of interest

The authors declare no conflict of interest.

Data availability

The relocated earthquake catalog used in this study is available upon reasonable request from the Gowa Geophysical Station, Agency for Meteorology, Climatology and Geophysics (BMKG). Sentinel-1 SAR data were obtained from the Alaska Satellite Facility (ASF) and are publicly available at http://search.asf.alaska.edu/.

References

Adam, L., Frehner, M., Sauer, K., Toy, V. & Guérin-Marthe, S. 2020. Seismic anisotropy and its impact on imaging the shallow alpine fault: an experimental and modeling perspective. *Journal of Geophysical Research: Solid Earth*, 125 (8). https://doi.org/10.1029/2019jb019029.

Arangio, S., Calò, F., Mauro, M. D., Bonano, M., Marsella, M. & Manunta, M. 2013. An application of the sbas-dinsar technique for the assessment of structural damage in the city of rome. *Structure and Infrastructure Engineering*, 10 (11): 1469–1483. https://doi.org/10.1080/15732479.2013.833949.

Asrurifak, M. 2010. Peta Respon Spektra Indonesia untuk Perencanaan Struktur Bangunan Tahan Gempa Berdasarkan Model Sumber Gempa Tiga Dimensi dalam Analisis Probabilitas [*Indonesian Spectral Response Map for Earthquake Resistant Building Structure Planning Based on Three-Dimensional Earthquake Source Model in Probability Analysis* – in Indonesian, with an English Abstract]. Doctoral Dissertation, Faculty of Civil Engineering, Bandung Institute of Technology, 278 pp.

Atzori, S. & Antonioli, A. 2011. Optimal fault resolution in geodetic inversion of coseismic data. *Geophysical Journal International*, 185 (1): 529-538. https://doi.org/10.1111/j.1365-246x.2011.04955.x.

Barros, L.D., Baques, M., Godano, M., Helmstetter, A., Deschamps, A., Larroque, C. & Courboulex, F. 2019. Fluid-induced swarms and coseismic stress transfer: a dual process highlighted in the aftershock sequence of the 7 april 2014 earthquake (ml 4.8, Ubaye, France). *Journal of Geophysical Research: Solid Earth*, 124 (4): 3918–3932. https://doi.org/10.1029/2018jb017226.

Billings, S.D. 1994. Simulated annealing for earthquake location. *Geophysical Journal International*, 118 (3): 680–692 https://doi.org/10.1111/j.1365-246X.1994.tb03993.x.

BMKG. 2019. Katalog Gempabumi Signifikan dan Merusak 1821 [*Catalog of Significant and Damaging Earthquakes* – in Indonesian]. BMKG press, 431 pp.

BMKG. 2025. Data Online Pusat Database BMKG. (Online). BMKG. https://simora.bmkg.go.id/simora/web/page/shakemap_terkini. (Accessed: 1 February 2025).

BPBD. 2025. Laporan kejadian gempa bumi tektonik di wilayah Kabupaten Kolaka Timur, Propinsi Sulawesi Tenggara: Periode 24 Januari s/d 5 Februari 2025 [*Survey Report of tectonic earthquake events in East Kolaka Regency, Southeast Sulawesi Province: Period 24 January to 5 February 2025* – in Indonesian]. BPBD press, 108 pp.

Bratt, S.R. & Nagy, W. 1991. *The LocSAT Program*. Science Applications International Corporation (SAIC), San Diego, California.

Carboni, F., Porreca, M., Valerio, E., Mariarosaria, M., de Luca, C., Azzaro, S., Ercoli, M. & Barchi, M.R. 2022. Surface ruptures and off-fault deformation of the October 2016 central Italy earthquakes from DInSAR data. *Scientific Reports*, 12 (1): 3172. https://doi.org/10.1038/s41598-022-07068-9.

Castaldo, R., Novellis, V.D., Solaro, G., Pepe, S., Tizzani, P., Luca, C.D. & Lanari, R. 2017. Finite element modelling of the 2015 gorkha earthquake through the joint exploitation of dinsar measurements and geologic-structural information. *Tectonophysics*, 714–715: 125–132. https://doi.org/10.1016/j.tecto.2016.06.037.

Chen, C.W. & Zebker, H.A. 2002. Phase unwrapping for large SAR interferograms: Statistical segmentation and generalized network models. *IEEE Transactions on Geoscience and Remote Sensing*, 40 (8): 1709–1719. https://doi.org/10.1109/TGRS.2002.802453.

Clerici, N., Valbuena Calderón, C.A. & Posada, J.M. 2017. Fusion of sentinel-1a and sentinel-2A data for land cover mapping: A case study in the lower Magdalena region, Colombia. *Journal of Maps*, 13 (2): 718–726. https://doi.org/10.1080/17445647.2017.1372316.

Craig, T.J. 2019. Accurate Depth Determination for Moderate-Magnitude Earthquakes Using Global Teleseismic Data. *Journal of Geophysical Research: Solid Earth*, 124 (2): 1759–1780. https://doi.org/10.1029/2018JB016902.

Daniarsyad, G., Priyobudi, P., Cahyaningrum, A.P., Wibisono, D.G., Sriyanto, S.P.D., Rosid, A., Pranata, B., Gunawan, I., Fatchurochman, I. & Daryono, D. 2023. Analysis on the Causative Fault of the 2021 Mw 6.0 Tehoru Earthquake in the South Coast of Seram Island: A Preliminary Result. *E3S Web of Conferences*, 447, *The 15th of Aceh International Workshop and Expo on Sustainable Tsunami Disaster Recovery (The 15th AIWEST-DR 2023*). https://doi.org/10.1051/e3sconf/202344701020.

Danré, P., Garagash, D., Barros, L.D., Cappa, F. & Ampuero, J. 2024. Control of seismicity migration in earthquake swarms by injected fluid volume and aseismic crack propagation. *Journal of Geophysical Research: Solid Earth*, 129 (1): 1–21. https://doi.org/10.1029/2023jb027276.

Daryono, M.R. 2016. Paleoseismologi Tropis Indonesia Dengan Studi Kasus di Sesar Sumatra, Sesar Palukoro-Matano, dan Sesar Lembang [*Paleoseismology of Tropical Indonesia Cases study in Sumatran Fault, Palukoro-Matano Fault, and Lembang Fault* – in Indonesian, with an English Abstract]. Doctoral Dissertation, Earth Science Doctoral Programme, Bandung Institute of Technology, 208 pp.

De Alban, J.D.T., Connette, G.M., Oswald, P. & Webb, E.L. 2018. Combined Landsat and L-band SAR data improves land cover classification and change detection in dynamic tropical landscapes. *Remote Sensing*, 10 (2): 306. https://doi.org/10.3390/rs10020306.

Delogkos, E., Manzocchi, T., Childs, C., Camanni, G. & Roche, V. 2020. The 3D structure of a normal fault from multiple outcrop observations. *Journal of Structural Geology*, 136: 104009. https://doi.org/10.1016/j.jsg.2020.104009.

Di Luccio, F., Ventura, G., di Giovambattista, R., Piscini, A. & Cinti, F.R. 2010. Normal faults and thrusts reactivated by deep fluids: The 6 April 2009 Mw 6.3 L'Aquila earthquake, central Italy. *Journal of Geophysical Research: Solid Earth*, 115 (6): 5596–5596. https://doi.org/10.1029/2009JB007190.

Dunn, M., Horton, S., DeShon, H. & Powell, C. 2010. High-resolution earthquake relocation in the New Madrid seismic zone. *Seismological Research Letters*, 81 (2): 406–413. https://doi.org/10.1785/gssrl.81.2.406.

Elliott, J.R., Walters, R.J., England, P.C., Jackson, J.A., Li, Z. & Parsons, B. 2010. Extension on the Tibetan plateau: Recent normal faulting measured by InSAR and body wave seismology. *Geophysical Journal International*, 183 (2): 503–535. https://doi.org/10.1111/j.1365-246X.2010.04754.x.

ESA. 2012. *Sentinel-1: ESA's radar observatory mission for GMES operational services*. ESA Special Publication, 1, 1322.

Fang, J., Xu, C., Wen, Y., Wang, S., Xu, G., Zhao, Y. & Yi, L. 2019. The 2018 Mw 7.5 Palu earthquake: A supershear rupture event constrained by InSAR and broadband regional seismograms. *Remote Sensing*, 11 (11): 1330. https://doi.org/10.3390/rs11111330.

Fang, N., Luo, X., Shen, P., Xie, L., Liu, G., Wei, F., Jiang, K. & Xu, W. 2023. An enhanced spectral diversity coregistration method for dual-polarimetric Sentinel-1A/B TOPS data. *Geodesy and Geodynamics*, 14 (5): 431–437. https://doi.org/10.1016/j.geog.2023.02.003.

Ferretti, A., Monti-Guarnieri, A., Prati, C. & Rocca, F. 2007a. *InSAR Principles (part A): Guidelines for SAR Interferometry Processing and Interpretation*. ESA Publications, TM-19A. ISBN 92-9092-233-8.

Ferretti, A., Monti-Guarnieri, A., Prati, C. & Rocca, F. 2007b. *InSAR processing: a practical approach (Part B)*. InSAR Principles: Guidelines for SAR Interferometry Processing and Interpretation. ESA Publications, TM-19B. ISBN 92-9092-233-8.

Fielding, E. J., Sladen, A., Li, Z., Avouac, J. P., Bürgmann, R. & Ryder, I. 2013. Kinematic fault slip evolution source models of the 2008 M7.9 Wenchuan earthquake in China from SAR interferometry, GPS and teleseismic analysis and implications for longmen shan tectonics. *Geophysical Journal International*, 194 (2): 1138–1166. https://doi.org/10.1093/gji/ggt155.

Fukushima, Y. & Ishimura, D. 2020. Characteristics of secondary-ruptured faults in the Aso caldera triggered by the 2016 mw 7.0 Kumamoto earthquake. *Earth, Planets and Space*, 72 (1): 175. https://doi.org/10.1186/s40623-020-01306-y.

Goebel, T., Hosseini, S. M., Cappa, F., Hauksson, E., Ampuero, J., Aminzadeh, F. & Saleeby, J.B. 2016. Wastewater disposal and earthquake swarm activity at the southern end of the Central Valley, California. *Geophysical Research Letters*, 43 (3): 1092–1099. https://doi.org/10.1002/2015gl066948.

Goldstein, R.M. & Werner, C.L. 1998. Radar interferogram filtering for geophysical applications. *Geophysical Research Letters*, 25 (21): 4035–4038. https://doi.org/10.1029/1998GL900033.

Guglielmi, Y., Cappa, F. & Amitrano, D. 2008. High-definition analysis of fluid-induced seismicity related to the mesoscale hydromechanical properties of a fault zone. *Geophysical Research Letters*, 35 (6): 1–6. https://doi.org/10.1029/2007gl033087

Hall, R. 2002. Cenozoic geological and plate tectonic evolution of SE Asia and the SW Pacific: Computer-based reconstructions, model and animations. *Journal of Asian Earth Sciences*, 20 (4). https://doi.org/10.1016/S1367-9120(01)00069-4.

Hall, R. 2019. The subduction initiation stage of the wilson cycle. *Geological Society Special Publication*, 470 (1): 415–437. https://doi.org/10.1144/SP470.3.

Hanka, W., Saul, J., Weber, B., Becker, J. & Harjadi, P. 2010. Real-time earthquake monitoring for tsunami warning in the Indian Ocean and beyond. *Natural Hazards and Earth System Science*, 10 (12): 2611–2622. https://doi.org/10.5194/nhess-10-2611-2010.

Hanssen, R.F. 2001. *Radar Interferometry: Data Interpretation and Error Analysis* (*Remote Sensing and Digital Image Processing*). Springer Dordrecht, 308 pp.

Hanssen, R.F. 2002. *Data interpretation and error analysis*. Kluwer Acaademic Publishers, 91 (5): 308pp.

Hasrul, H., Hasria, H., & Asfar, S. 2021. Studi geomorfologi Daerah Samaturu, Kabupaten Kolaka, Provinsi Sulawesi Tenggara [*Geomorphological study of Samaturu area, Kolaka Regency, Southeast Sulawesi Province* - in Indonesian]. *OPHIOLITE: Jurnal Geologi Terapan*, 2 (1): 45–58. https://doi.org/10.56099/ophiolite.v2i1.11410.

Heimann, S. 2011. *A robust method to estimate kinematic earth quake source parameters*. Ph.D Thesis, Department of Geosciences, University of Hamburg, 151pp.

Howarth, J.D., Cochran, U.A., Langridge, R.M., Clark, K., Fitzsimons, S.J., Berryman, K., Villamor, P. & Strong, D.T. 2018. Past large earthquakes on the Alpine Fault: paleoseismological progress and future directions. *New Zealand Journal of Geology and Geophysics,* 61 (3): 309–328. https://doi.org/10.1080/00288306.2018.1464658.

Hu, L., Dai, K., Xing, C., Li, Z., Tomás, R., Clark, B., Shi, X., Chen, M., Zhang, R., Qiu, Q. & Lu, Y. 2019. Land subsidence in Beijing and its relationship with geological faults revealed by Sentinel-1 InSAR observations. *International Journal of Applied Earth*

Observation and Geoinformation, 82: 101886. https://doi.org/10.1016/j.jag.2019.05.019.

Huesca-Pérez, E., Valenzuela, R.W. & Ortega, R. 2016. Crustal anisotropy from tectonic tremor in Guerrero, Mexico. *Geochemistry, Geophysics, Geosystems*, 17 (6): 2323–2335. https://doi.org/10.1002/2016GC006358.

Hutchings, S.J. & Mooney, W.D. 2021. The Seismicity of Indonesia and Tectonic Implications. *Geochemistry, Geophysics, Geosystems*, 22 (9): 1–44. https://doi.org/10.1029/2021GC009812.

Irsyam, M., Cummins, P.R., Asrurifak, M., Faizal, L., Natawidjaja, D.H., Widiyantoro, S., Meilano, I., Triyoso, W., Rudiyanto, A., Hidayati, S., Ridwan, M., Hanifa, N.R. & Syahbana, A.J. 2020. Development of the 2017 national seismic hazard maps of Indonesia. *Earthquake Spectra*, 36 (1): 112–136. https://doi.org/10.1177/8755293020951206.

Kennett, B.L.N. & Engdahl, E.R. 1991. Traveltimes for global earthquake location and phase identification. *Geophysical Journal International*, 105 (2). https://doi.org/10.1111/j.1365-246X.1991.tb06724.x.

Kennett, B.L.N., Engdahl, E.R. & Buland, R. 1995. Constraints on seismic velocities in the Earth from traveltimes. *Geophysical Journal International*, 122 (1): 108–124. https://doi.org/10.1111/j.1365-246X.1995.tb03540.x.

Kim, W. 2013. Induced seismicity associated with fluid injection into a deep well in Youngstown, Ohio. *Journal of Geophysical Research: Solid Earth*, 118 (7): 3506–3518. https://doi.org/10.1002/jgrb.50247.

Lee, S.-J., Yun, H. & Kim, T. 2025. Monitoring of High-Speed Railway Ground Deformation Using Interferometric Synthetic Aperture Radar Image Analysis. *Applied Sciences*, 15 (8): 4318. https://doi.org/10.3390/app15084318.

Li, Z., Elliott, J.R., Feng, W., Jackson, J.A., Parsons, B.E. & Walters, R.J. 2011. The 2010 MW 6.8 Yushu (Qinghai, China) earthquake: Constraints provided by InSAR and body wave seismology. *Journal of Geophysical Research: Solid Earth*, 116 (10): 1–16. https://doi.org/10.1029/2011JB008358.

Liu, X., Zhao, C., Zhang, Q., Lu, Z. & Li, Z. 2020. Deformation of the Baige Landslide, Tibet, China, Revealed Through the Integration of Cross-Platform ALOS/PALSAR-1 and ALOS/PALSAR-2 SAR Observations. *Geophysical Research Letters*, 47 (3): 1–8. https://doi.org/10.1029/2019GL086142.

Luebeck, D., Wimmer, C., Moreira, L.F., Alcântara, M., Oré, G., Góes, J.A., Oliveira, L.P., Teruel, B., Bins, L.S., Gabrielli, L.H. & Hernandez-Figueroa, H.E. 2020. Drone-borne differential SAR interferometry. *Remote Sensing*, 12 (5): 778. https://doi.org/10.3390/rs12050778.

Mamot, P., Weber, S., Lanz, M. & Krautblatter, M. 2020. Brief communication: The influence of mica-rich rocks on the shear strength of ice-filled discontinuities. *Cryosphere*, 14 (6): 1849–1855. https://doi.org/10.5194/tc-14-1849-2020.

Mancini, F., Grassi, F. & Cenni, N. 2021. A Workflow Based on SNAP–StaMPS Open-Source Tools and GNSS Data for PSI-Based Ground Deformation Using Dual-Orbit Sentinel-1 Data: Accuracy Assessment with Error Propagation Analysis. *Remote Sensing*, 13 (4): 753. https://doi.org/10.3390/rs13040753.

Manzo, M., Fialko, Y., Casu, F., Pepe, A. & Lanari, R. 2011. A quantitative assessment of dinsar measurements of interseismic deformation: the southern san andreas fault case study. *Pure and Applied Geophysics*, 169 (8): 1463–1482. https://doi.org/10.1007/s00024-011-0403-2.

Markogiannaki, O., Karavias, A., Bafi, D., Angelou, D. & Parcharidis, I. 2020. A geospatial intelligence application to support post-disaster inspections based on local exposure information and on co-seismic DInSAR results: the case of the Durres (Albania) earthquake on November 26, 2019. *Natural Hazards*, 103 (3): 3085–3100. https://doi.org/10.1007/s11069-020-04120-7.

McGarr, A. 2014. Maximum magnitude earthquakes induced by fluid injection. *Journal of Geophysical Research: Solid Earth*, 119 (2): 1008–1019. https://doi.org/10.1002/2013jb010597.

McGarragh, G., Poulsen, C., Povey, A., Thomas, G., Christensen, M., Sus, O., Schlundt, C., Stapelberg, S., Stengel, M., Grainger, D., McGarragh, G., Poulsen, C., Povey, A., Thomas, G., Christensen, M., Sus, O., Schlundt, C., Stapelberg, S., Stengel, M. & Grainger, D. 2015. *SNAP (Sentinel Application Platform) and the ESA Sentinel 3 Toolbox*. ESASP, 734.

Meyer, M.G. & Sahr, J.D. 2004. Passive coherent scatter radar interferometer implementation, observations, and analysis. *Radio Science*, 39 (3): 1–10. https://doi.org/10.1029/2003RS002985.

Minson, S.E., Baltay, A.S., Cochran, E.S., McBride, S.K. & Milner, K.R. 2020. Shaking is almost always a surprise: The earthquakes that produce significant ground motion. *Seismological Research Letters*, 92 (1): 460–468. https://doi.org/10.1785/0220200165.

Natawidjaja, D.H. 2021. Riset Sesar Aktif Indonesia dan Peranannya dalam Mitigasi Bencana Gempa dan Tsunami [*Research on Indonesia's Active Faults and Their Role in Earthquake and Tsunami Disaster Mitigation* – in Indonesian]. LIPI Press, 95pp. https://doi.org/10.14203/press.400.

Natawidjaja, D.H., Daryono, M.R., Prasetya, G., Udrekh Liu, P.L.F., Hananto, N.D., Kongko, W., Triyoso, W., Puji, A.R., Meilano, I., Gunawan, E., Supendi, P., Pamumpuni, A., Irsyam, M., Faizal, L., Hidayati, S., Sapiie, B., Kusuma, M.A. & Tawil, S. 2021. The 2018 Mw7.5 Palu "supershear" earthquake ruptures geological fault's multisegment separated by large bends: Results from integrating field measurements, LiDAR, swath bathymetry and seismic-reflection data. *Geophysical Journal International*, 224 (2): 985–1002. https://doi.org/10.1093/gji/ggaa498.

Nedelcu, S. & Brisco, B. 2018. Comparison between Range-Doppler and Rational-Function methods for SAR Terrain Geocoding. *Canadian Journal of Remote Sensing*, 44 (3): 191–201. https://doi.org/10.1080/07038992.2018.1479635.

Oliva-Urcia, B., Casas, A.M., Ramón, M.J., Leiss, B., Mariani, E. & Román-Berdiel, T. 2012. On the reliability of AMS in ilmenite-type granites: An insight from the Marimanha pluton, central Pyrenees. *Geophysical Journal International*, 189 (1): 187–203. https://doi.org/10.1111/j.1365-246X.2011.05355.x.

Pailoplee, S., Sugiyama, Y. & Charusiri, P. 2009. Deterministic and probabilistic seismic hazard analyses in Thailand and adjacent areas using active fault data. *Earth, Planets and Space*, 61 (12): 1313–1325. https://doi.org/10.1186/BF03352984.

Pasari, S., Simanjuntak, A.V.H., Neha & Sharma, Y. 2021. Nowcasting earthquakes in Sulawesi Island, ndonesia. *Geoscience Letters*, 8 (1): 27. https://doi.org/10.1186/s40562-021-00197-5.

Philibosian, B. & Meltzner, A.J. 2020. Segmentation and supercycles: A catalog of earthquake rupture patterns from the Sumatran Sunda Megathrust and other well-studied faults worldwide. *Quaternary Science Reviews*, 241. https://doi.org/10.1016/j.quascirev.2020.106390.

Purba, J., Harisma, H., Priadi, R., Amelia, R., Dwilyantari, A.A.I., Jaya, L.M.G., Restele, L.O. & Putra, I.M.W.G. 2024a. Surface deformation and its implications for land degradation after the 2021 Flores earthquake (M7.4) using differential interferometry synthetic aperture radar. *Journal of Degraded and Mining Lands Management*, 12 (1): 6819–6831. https://doi.org/10.15243/jdmlm.2024.121.6819.

Purba, J., Restele, L.O., Hadini, L.O., Usman, I., Hasria, H. & Harisma, H. 2024b. Spatial study of seismic hazard using classical probabilistic seismic hazard analysis (PSHA) method in the Kendari city area. *Indonesian Physical Review*, 7 (3): 300–318. https://doi.org/10.29303/ipr.v7i3.325.

Purba, J., Yulinda, R., Pertiwi, I.I. & Saadia, A.O. 2025a. Seismic hazard analysis in Malang Raya through classical PSHA method using OpenQuake with spatial approach. JAGAT. *Jurnal Geografi Aplikasi dan Teknologi*, 9 (1): 1–14. https://doi.org/10.13117/jagat.9.1.1.

Purba, S.M., Alyssa, Y.F., Nadia, M., Asra, N. & Muksin, U. 2025b. The influence of seismometer coverage on the earthquake focal mechanism solution (case study: toba swarm earthquake). *IOP Conference Series: Earth and Environmental Science*, 1479 (1): 012014. https://doi.org/10.1088/1755-1315/1479/1/012014.

PuSGeN. 2017. Peta Sumber dan Bahaya Gempa Indonesia Tahun 2017 [*Map of Indonesia Earthquake Sources and Hazards in 2017*- in Indonesian]. PUPR Press, 76 pp.

PuSGeN. 2022. Peta Deagregasi Bahaya Gempa Indonesia Untuk Perencanaan Dan Evaluasi Infrastruktur Tahan Gempa [*Indonesia Earthquake Hazard Deaggregation Map for Earthquake Resistant Infrastructure Planning and Evaluation* – in Indonesian]. PUPR Press, 386 pp.

PuSGeN. 2024. Peta Sumber dan Bahaya Gempa Indonesia Tahun 2024 [*Map of Indonesia Earthquake Sources and Hazards in 2024* – in Indonesian]. PUPR Press, 515 pp.

Richards, J.A. 2009. Erratum to: Remote Sensing with Imaging Radar. In: Remote Sensing with Imaging Radar. *Signals and Communication Technology*. Springer, Berlin, Heidelberg. https://doi.org/10.1007/978-3-642-02020-9-10.

Rocca, F., Ferretti, A., Monti-Guarnieri, A.V., Prati, C.M. & Massonnet, D. 2007. InSAR processing: a mathematical approach (Part C). *InSAR Principles: Guidelines for SAR Interferometry Processing and Interpretation*.

Roselli, P., Agostinetti, N.P. & Braun, T. 2010. Shear-velocity and anisotropy structure of a retreating extensional forearc (tuscany, italy) from receiver functions inversion. *Geophysical Journal International*, 181 (1): 545–556. https://doi.org/10.1111/j.1365-246x.2010.04520.x.

Scholz, C.H. 2019. *The Mechanics of Earthquakes and Faulting*. The Mechanics of Earthquakes and Faulting, 3rd Edition.https://doi.org/10.1017/9781316681473.

Serhalawan, Y. & Chen, P.-F. 2024. Seismotectonics of Sulawesi, Indonesia. *Tectonophysics*, *883*, 230366. https://doi.org/https://doi.org/10.1016/j.tecto.2024.230366.

Silva, V., Amo-Oduro, D., Calderón, A., Costa, C., Dabbeek, J., Despotaki, V., Martins, L., Pagani, M., Rao, A., Simionato, M., Viganò, D., Yepes-Estrada, C., Acevedo, A. B., Crowley, H., Horspool, N., Jaiswal, K., Journeay, M. & Pittore, M. 2020. Development of a Global Seismic Risk Model. *Earthquake Spectra*, 36 (1): 372–394. https://doi.org/10.1177/8755293019899953.

Simandjuntak, T.O., Surono, dan Supandjono, J.B. 1993. Peta Geologi Lembar Kolaka, Sulawesi Tenggara [*Geological Map of Kolaka Sheet, Southeast Sulawesi*]. Pusat Penelitian dan Pengembangan Geologi, Bandung. (in Indonesian).

Soehaimi, A., Sopyan, Y., Ma'mur., Agustin, F. 2022. Peta Patahan Aktif Indonesia [*Map of Active Faults in Indonesia* – in Indonesian]. Pusat Survey Geologi, Bandung.

Sreejith, K.M., Sunil, P.S., Agrawal, R., Saji, A. P., Ramesh, D. S., & Rajawat, A.S. 2016. Coseismic and early postseismic deformation due to the 25 April 2015, Mw 7.8 Gorkha, Nepal, earthquake from InSAR and GPS measurements. *Geophysical Research Letters*, 43 (7): 3160–3168. https://doi.org/10.1002/2016GL067907.

Stallard, A. & Shelley, D. 2005. The initiation and development of metamorphic foliation in the Otago Schist, Part 1: Competitive oriented growth of white mica. *Journal of Metamorphic Geology*, 23 (6): 425–442. https://doi.org/10.1111/j.1525-1314.2005.00587.x.

Supendi, P., Nugraha, A.D., Widiyantoro, S., Abdullah, C.I., Puspito, N.T., Palgunadi, K.H., Daryono, D. & Wiyono, S.H. 2019. Hypocenter relocation of the aftershocks of the Mw 7.5 Palu earthquake (September 28, 2018) and swarm earthquakes of Mamasa, Sulawesi, Indonesia, using the BMKG network data. *Geoscience Letters*, 6 (1): 1–11. https://doi.org/10.1186/s40562-019-0148-9.

Supendi, P., Nugraha, A.D., Widiyantoro, S., Pesicek, J.D., Thurber, C.H., Abdullah, C.I., Daryono, D., Wiyono, S.H., Shiddiqi, H.A. & Rosalia, S. 2020. Relocated aftershocks and background seismicity in eastern Indonesia shed light on the 2018 Lombok and Palu earthquake sequences. *Geophysical Journal International*, 221 (3): 1845–1855. https://doi.org/10.1093/gji/ggaa118.

Supendi, P., Rawlinson, N., Prayitno, B.S., Sianipar, D., Simanjuntak, A., Widiyantoro, S., Palgunadi, K.H., Kurniawan, A., Shiddiqi, H.A., Nugraha, A.D., Sahara, D.P., Daryono, D., Triyono, R., Adi, S. P., Karnawati, D., Daniarsyad, G., Ahadi, S., Fatchurochman, I., Anugrah, S.D., Heryandoko, N. & Sudrajat, A. 2023. A previously unidentified fault revealed by the February 25, 2022 (Mw 6.1) Pasaman Earthquake, West Sumatra, Indonesia. *Physics of the Earth and Planetary Interiors*, 334: 1–10. https://doi.org/10.1016/j.pepi.2022.106973.

Supendi, P., Rawlinson, N., Prayitno, B.S., Widiyantoro, S., Simanjuntak, A., Palgunadi, K. H., Kurniawan, A., Marliyani, G.I., Nugraha, A.D., Daryono, D., Anugrah, S.D., Fatchurochman, I., Gunawan, M.T., Sadly, M., Adi, S.P., Karnawati, D. & Arimuko, A. 2022. The Kalaotoa Fault: A Newly Identified Fault that Generated the Mw 7.3 Flores Sea Earthquake. *Seismic Record*, 2 (3): 176–185. https://doi.org/10.1785/0320220015.

Surono & Bachri, S. 2002. Stratigraphy, sedimentation and palaeogeographic significance of the Triassic Meluhu Formation, Southeast arm of Sulawesi, Eastern Indonesia. *Journal of Asian Earth Sciences*, 20 (2): 177–192. https://doi.org/10.1016/S1367-9120(01)00037-2.

Surono, 2010. Geologi Sulawesi. LIPI Press, Indonesia, 349 pp, (in Indonesian).

Surono, 2013. Geologi Lengan Tenggara Sulawesi [*Geology of the Southeastern Arm of Sulawesi* – in Indonesian]. Badan Geologi, Kementerian Energi dan Sumber Daya Mineral Press, 177 pp.

Tolomei, C., Caputo, R., Polcari, M., Famiglietti, N.A., Maggini, M. & Stramondo, S. 2021. The use of interferometric synthetic aperture radar for isolating the contribution of major shocks: The case of the march 2021 thessaly, greece, seismic sequence. *Geosciences*, 11 (5): 191. https://doi.org/10.3390/geosciences11050191.

Waldhauser, F. 2001. *HypoDD: A computer program to compute double-difference hypocenter locations.* U.S. Geol. Surv. Open File Rep., 01–113.

Waldhauser, F. & Schaff, D.P. 2007. Regional and teleseismic double-difference earthquake relocation using waveform cross-correlation and global bulletin data. *Journal of Geophysical Research: Solid Earth*, 112 (B12). https://doi.org/10.1029/2007jb004938.

Waldhauser, F. & Ellsworth, W.L. 2000. A Double-difference Earthquake location algorithm: Method and application to the Northern Hayward Fault, California. *Bulletin of the Seismological Society of America*, 90 (6): 1353–1368. https://doi.org/10.1785/0120000006.

Wang, Z., Zhang, R. & Liu, Y. 2019. 3D coseismic deformation field and source parameters of the 2017 iran-iraq

mw7.3 earthquake inferred from DINSAR and MAI measurements. *Remote Sensing*, 11 (19): 2248. https://doi.org/10.3390/rs11192248.

Waqas, U., Qureshi, M.U., Saqib, S., Rashid, H.M.A. & Rasool, A.M. 2024. Evaluation of strength anisotropy in foliated metamorphic rocks: a review focused on microscopic mechanisms. *Geosciences*, 14 (10): 253. https://doi.org/10.3390/geosciences14100253.

Watkinson, I.M. & Hall, R. 2017. Fault systems of the eastern Indonesian triple junction: Evaluation of Quaternary activity and implications for seismic hazards. *Geological Society Special Publication*, 441 (1): 71–120. https://doi.org/10.1144/SP441.8.

Wells, D.L. & Coppersmith, K.J. 1994. New empirical relationships among magnitude, rupture length, rupture width, rupture area, and surface displacement. *Bulletin - Seismological Society of America*, 84 (4): 974–1002. https://doi.org/10.1785/bssa0840040974.

White, L.T., Hall, R. & Armstrong, R. 2014. The age of undeformed dacite intrusions within the kolaka fault zone, se sulawesi, indonesia. Journal of Asian Earth Sciences, 94, 105-112. https://doi.org/10.1016/j.jseaes.2014.08.014.

Wijayanto, I., Fatchurochman, I., Pranata, B., Gunawan, I., Supendi, P., Daryono, N., Riama, N.F. & Karnawati, D. 2025. Analisis rangkaian gempabumi Kolaka, Sulawesi Tenggara. [*Analysis of the Kolaka earthquake sequence, Southeast Sulawesi* – in Indonesian]. Badan Meteorologi, Klimatologi, dan Geofisika. https://www.bmkg.go.id/artikel/analisis-rangkaian-gempabumi-kolaka-sulawesi-tenggara-tanggal-3-29-januari-2025.

Wu, G., Kim, Y.S., Su, Z., Yang, P., Ma, D. & Zheng, D. 2020. Segment interaction and linkage evolution in a conjugate strike-slip fault system from the Tarim Basin, NW China. *Marine and Petroleum Geology*, 112: 104054. https://doi.org/10.1016/j.marpetgeo.2019.104054.

Xu, C., Liu, Y., Wen, Y. & Wang, R. 2010. Coseismic slip distribution of the 2008 mw 7.9 Wenchuan earthquake from joint inversion of GPS and InSAR data. *Bulletin of the Seismological Society of America*, 100 (5 B). https://doi.org/10.1785/0120090253.

Xu, Y., Li, T., Tang, X., Zhang, X., Fan, H. & Wang, Y. 2022. Research on the Applicability of DInSAR, Stacking-InSAR and SBAS-InSAR for Mining Region Subsidence Detection in the Datong Coalfield. *Remote Sensing*, 14 (14): 3314. https://doi.org/10.3390/rs14143314.

Yoshida, K. & Hasegawa, A. 2018. Hypocenter migration and seismicity pattern change in the Yamagata-Fukushima border, ne japan, caused by fluid movement and pore pressure variation. *Journal of Geophysical Research: Solid Earth*, 123 (6): 5000–5017. https://doi.org/10.1029/2018jb015468.

Zebker, H.A. & Goldstein, R.M. 1986. Topographic mapping from interferometric synthetic aperture radar observations. *Journal of Geophysical Research: Solid Earth*, 91 (B5): 4993–4999. https://doi.org/https://doi.org/10.1029/JB091iB05p04993

Zhang, L., Balz, T. & Liao, M. 2012. Satellite SAR geocoding with refined RPC model. ISPRS *Journal of Photogrammetry and Remote Sensing*, 69: 37–49. https://doi.org/10.1016/j.isprsjprs.2012.02.004.

Zhang, Y., Fadugba, O., Powell, C., Horton, S. & Langston, C.A. 2022. A New Madrid Seismic Zone Fault System Model from Relative Event Locations and Application of Optimal Anisotropic Dynamic Clustering. *Journal of Geophysical Research: Solid Earth*, 127 (10): 1–18. https://doi.org/10.1029/2022JB024194

Резиме

Расед Purpri: Новоидентификовани активни расед у Источној Колаки, Индонезија (на основу HypoDD и DInSAR)

Овај рад представља идентификацију и карактеризацију Purpri раседа, претходно немапираног активног раседа у Источној Колаки, Индонезија. Кроз интеграцију сеизмичког премештања коришћењем HypoDD методе и анализе деформације тла из Sentinel-1A DInSAR података, показано је да је Purpri расед независна сеизмогена структура, различита од утврђеног система раседа Колака. Расед показује механизам косо-нормалног померања, који прилагођава и екстензионално и левобочно кретање, са сеизмичношћу претежно концентрисаном у плиткој кори (дубина <10 km).

Површинско померање изведено из DInSAR -а, обележено слегањем на западном блоку (-13 cm) и издизањем на источном блоку (+11 cm), просторно одговара премештеној сеизмичности, појачавајући тумачење да расед активно

ослобађа акумулирани напон. Кохерентност између сеизмолошких и геодетских посматрања потврђује структурни и тектонски значај Purpri раседа унутар регионалног режима напрезања.

Препознавање овог раседа има важне импликације за процене сеизмичког ризика у југоисточном Сулавесију, јер тренутно није присутан у постојећим регионалним моделима раседа. Његова плитка сеизмичка активност и капацитет за значајне површинске деформације указују на висок потенцијал за умерене до јаке земљотресе, што наглашава потребу за његовим укључивањем у ажуриране оквире опасности.

Будућа истраживања требало би да дају приоритет моделовању сеизмичке брзине високе резолуције, континуираном GPS и InSAR праћењу, палеосеизмолошком истраживању ровова и нумеричким симулацијама руптура како би се усавршила кинематика раседа, интервали понављања и потенцијал стварања рутура. Ова студија показује важност интегрисања вишеструких геофизичких техника у карактеризацији раседа и наглашава потребу за проактивним проценама сеизмичког ризика како би се побољшала припремљеност за земљотресе и стратегије за ублажавање ризика од катастрофа у југоисточном Сулавесију.

Manuscript received April 17, 2025
Revised manuscript accepted June 02, 2025